PERGAMON

International Journal of Heat and Mass Transfer 44 (2001) 4035–4046

International Journal of HEAT and MASS TRANSFER

www.elsevier.com/locate/ijhmt

Thermal phase lag in a solid containing periodic planar cracks

John R. Dryden [a,*], Frank Zok [b]

[a] *Department of Mechanical and Materials Engineering, University of Western Ontario, London, Ont., Canada N6A 5B9*
[b] *Materials Department, University of California, Santa Barbara, CA 93106, USA*

Received 5 January 2000; received in revised form 9 January 2001

Abstract

The thermal response of a solid containing a periodic planar array of cracks is considered. Special emphasis is placed on the extra phase lag of the thermal wave due to each crack when the solid is heated by a periodic point source. An exact solution for this phase lag is obtained in the form of an integral that requires numerical evaluation. Additionally, simpler asymptotic solutions are obtained for both low and high heating frequencies and their validity ranges are determined through comparisons with the exact numerical results. Furthermore, comparisons are made with the prediction of an equivalent solid model wherein the effective thermal conductivity perpendicular to the cracks is obtained through a simple resistance summation procedure. It is demonstrated that the extra phase lag due to each crack reaches a constant value (independent of location) at distances from the heat source that are greater than about five times the crack spacing. In most cases, the variation in the phase lag with frequency and the thermal properties of both the solid and the cracks is accurately described by the asymptotic solutions.

1. Introduction

Photothermal techniques are used extensively for the determination of the thermal properties of materials [1–3]. In this context, an optical energy source such as a laser is used to heat the material in a prescribed manner (typically as a short duration pulse or as a continuous modulated wave) and the temporal and spatial distributions of temperature are measured using any one of a variety of measurement devices. An especially popular version is the so-called laser flash method, wherein a high-powered laser is used to produce a pulse over a large area of the specimen surface and the time-dependent temperature profile is then measured on the back-side of the specimen by an infra-red camera. In comparison with the flash method, it is possible to continuously modulate the input flux over a large area of the specimen surface so that a planar thermal wave is driven into the solid. On the incident surface, both the magnitude of the wave and the phase lag between the temperature and the flux, can be measured. Using these two measurements, in conjunction with an analytical solution, it is possible to deduce the unknown thermophysical properties of a layer that is bonded onto a substrate of material having known properties [3]. An alternate version involves the use of a focused laser to produce a modulated heat source that acts essentially at a point on the surface and measurement of the phase lag of the temperature with respect to the input heat at some other location on the surface, using either a thermocouple or an infra-red sensor along with a lock-in amplifier. The latter technique is preferred for measuring material properties on a finer size scale, making it particularly attractive for use with new developmental materials that are available only in limited sizes or for probing local variations in properties due to microstructural heterogeneities. It has also proved to be useful for measuring the thermal conductance of cracks and interfaces [4–6]. Regardless of the details of the measurement method, an analysis of the heat flow behavior is invariably required for the interpretation of the measurements and the determination of the relevant thermal properties.

The focus of the present paper is on the interaction of a periodic thermal wave with an array of equally-spaced planar cracks or interfaces in an otherwise homogeneous

* Corresponding author. Tel.: +1-519-661-211 ext. 88307; fax: +1-519-661-3020.
E-mail address: jdryden@engga.uwo.ca (J.R. Dryden).

0017-9310/01/$ - see front matter
PII: S0017-9310(01)00049-7

Nomenclature

a	spacing between cracks
$\mathscr{C}$	cell transition matrix (Eq. (17))
h_c	thermal conductance across the crack
k	thermal conductivity of the pristine material
k_z	conductivity in the z direction after cracking (Eq. (2))
$m^2 = i\omega/\alpha$	real part of m is the penetration depth (Eq. (10))
$p = \sqrt{a^2\omega/2\alpha}$	dimensionless frequency (Eq. (4))
$T(r,z,t)$	temperature (Eq. (6))
$T(n)$	temperature at $z = na$ (Eq. (26))
$X_e = \phi_e - \phi_0$	extra lag across cell according to equivalent solid model (Eq. (5))
$X(n) = \phi_n - \phi_0$	extra lag across nth cell according to exact solution (Eq. (28))
$X = \phi_\infty - \phi_0$	asymptotic limit for the extra lag as $n \to \infty$ (Eq. (32))
$X_\ell = \phi_\ell - \phi_0$	extra lag predicted by the low frequency model (Eq. (43))
X_i	extra lag according to the non-interacting model (Eq. (53))

Greek symbols

$\alpha = k/\rho C_p$	thermal diffusivity of the pristine solid
α_z	thermal diffusivity of the cracked solid (Eq. (55))
β	Hankel transform parameter (Eq. (11))
$\gamma = \sqrt{\beta^2 + m^2}$	root of transformed heat equation ((12))
ϵ	characteristic root of difference equation ((38))
ζ, η and θ	elements of $\mathscr{C}$ (Eq. (18))
μ and μ^{-1}	the two eigenvalues of $\mathscr{C}$ (Eq. (20))
$v = \sqrt{\eta/\theta}$	parameter in $\mathscr{C}^n$ (Eq. (23))
$\rho_c = k/ah_c$	dimensionless interface resistance (Eq. (1))
ϕ	phase lag over a distance a in cracked solid
ϕ_0	phase lag over a distance a in pristine solid
$\omega = 2\pi f$	frequency of the source

solid. The objective is to calculate the phase lag that occurs across each crack in terms of the thermal properties of the solid and the cracks, the frequency of heating, and the position within the solid. The work is motivated by concurrent experimental studies on the thermal diffusivity of fiber-reinforced ceramic composites subject to tensile stressing [7]. Upon application of stress along the fiber direction, these materials exhibit multiple matrix cracks transverse to the loading direction, with each crack bridged by fibers. The cracks are essentially planar in nature and their spacing decreases with increasing applied stress. The goal here is to develop the requisite theoretical analysis for the interpretation of phase lag measurements made along the loading axis (perpendicular to the cracks), allowing determination of the thermal conductance of each of the cracks. The analysis presented here is also applicable to other materials systems containing multiple interfaces such as multilayered structures found in electronic devices. Although not explored explicitly in this paper, the analysis can be further used to draw insights into the thermal response of materials containing cracks with finite lengths and with a distribution in orientations.

2. Preliminaries and objectives

The composite in its "pristine" uncracked condition has thermal properties that are assumed to be isotropic with thermal conductivity k. The application of stress generates multiple cracks, each of which is perpendicular to the tensile axis, so that from a macroscopic viewpoint the solid is rendered anisotropic. In the analysis, it is convenient to use a cylindrical coordinate system (r,z) with the z axis perpendicular to the cracks and a periodic point source acts at the origin as shown in Fig. 1(a). The first unit cell is shown in Fig. 1(b) and is configured so that the crack is located at the midpoint of the cell; the crack has a thermal conductance h_c. The resistance per area of the crack is equal to $1/h_c$ and the resistance of the solid is a/k. The dimensionless quantity

$$\rho_c = \frac{k}{ah_c} \tag{1}$$

represents the ratio of the thermal resistance of the crack to that of the solid, and ρ_c is the reciprocal of the Biot number. The heat flow q across the crack is continuous. In contrast, there is a temperature discontinuity ΔT across the crack that is given by $\Delta T = q/h_c$.

2.1. Equivalent anisotropic solid

For one-dimensional flow in the z direction the effective thermal conductivity k_z is somewhat reduced and is given by

$$k_z = \frac{k}{1+\rho_c}. \tag{2}$$

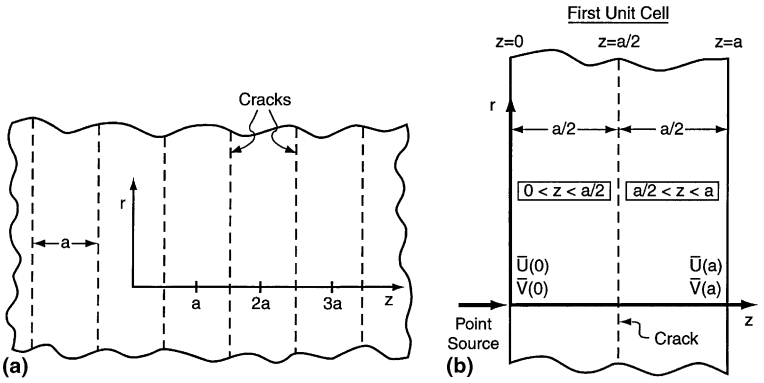

Fig. 1. (a) Idealized model of the composite after application of uniaxial stress in the z direction. The crack spacing is equal to "a" and k_z is the effective conductivity in the z direction. The periodic point source acts at the origin. (b) The first unit cell $0 < z < a$ showing the crack at $z = a/2$. The state transition matrix $\mathscr{C}$ relates $\{\overline{U}(0), \overline{V}(0)\}$ to $\{\overline{U}(a), \overline{V}(a)\}$.

In contrast, the radial and tangential conductivities remain unchanged. Thus, the "equivalent" anisotropic solid corresponding to the cracked composite has a thermal conductivity tensor k_{ij} given by

$$k_{ij} = \begin{pmatrix} k & 0 & 0 \\ 0 & k & 0 \\ 0 & 0 & k_z \end{pmatrix}. \tag{3}$$

This result for k_{ij} is essentially based upon the method described over a century ago by James Clerk Maxwell [8] for finding the average properties of stratified material. More recently [9,10], the same result for k_{ij} has been obtained using non-standard analysis. In essence, the result for k_z corresponds to an electrical analogue series circuit in which the thermal resistances are summed, i.e., for a unit area $a/k_z = a/k + 1/h_c$. Implicit in this circuit is the assumption that the heat flow is constant.

The equivalent solid model can be used to estimate the phase lag of a thermal wave when the heat is applied in a periodic manner. To begin, consider a periodic point source which is emitting heat in an infinite, pristine solid at a frequency $\omega = 2\pi f$. After periodic steady conditions are attained, the phase lag ϕ_0 measured over the distance a (the crack spacing), is given by [11]

$$\phi_0 = p, \tag{4}$$

where $p = a\sqrt{\omega/2\alpha}$ is dimensionless frequency and α is the thermal diffusivity of the pristine material. After the cracks have been introduced, the phase lag over the same distance "a" measured along the z axis is represented by ϕ and the *extra* lag X caused by the crack is then given by $X = \phi - \phi_0$. The attenuation of heat flow across the cell depends upon $\exp[-p]$ and at sufficiently low frequencies the attenuation is minimal. Under these conditions the thermal behaviour approaches steady-state and the overall microstructure acts as an equivalent solid with an effective diffusivity $\alpha_z = \alpha/(1 + \rho_c)$ in the z direction. The phase lag ϕ_e of this equivalent solid is $\phi_e = \phi_0\sqrt{1 + \rho_c}$, and the extra phase lag is

$$X_e = \phi_e - \phi_0 = \phi_0\left\{\sqrt{1 + \rho_c} - 1\right\}, \tag{5}$$

where the subscript "e" indicates the equivalent solid. In this treatment, the discrete microstructural features of the cell have been smoothed out and X_e corresponds to the phase lag as predicted by the homogeneous anisotropic solid model.

The attenuation of heat across the cell becomes larger as the frequency is increased and eventually the use of the equivalent solid model becomes unacceptable. The objectives of the present paper are to determine the phase lag in a cracked solid over a wide frequency range and to ascertain the limitations on the use of the equivalent solid model. The course of the paper proceeds as given below.

1. In Section 3, an exact analysis of the transient response of a unit cell is presented. The state transition matrix $\mathscr{C}$ which relates the thermal field across the cell is found. These matrices are cascaded to find the thermal response at any point within the solid. The temperature along the z axis is found and the extra lag across the cell $(n-1)a < z < na$ is designated $X(n)$. It is shown that:
   (a) the extra lag $X(n)$ across each cell approaches a constant limit rather quickly, and for $n > 5$ the extra lag $X(n) \to X$. Consequently, X is given special attention;
   (b) the extra lag X due to the crack initially increases linearly with p, as given in (5) but eventually becomes non-linear and, for large values of ρ_c, attains a maximum value.
2. In Section 4, a simplified model for the low frequency response, $p \ll 1$, is given. As in the case of the exact solution, the extra lag approaches an asymptotic value which is designated X_ℓ where the ℓ indicates

"low frequency." At sufficiently low frequencies, $X_\ell \sim X_e$. As p increases X_ℓ becomes non-linear and the maximum attainable extra lag caused by a crack is $\pi/2$.

3. In Section 5, the thermal behaviour associated with neglecting the secondary scattering is considered. This simplification is reasonable either at high frequency ($p \gg 1$), *or* if the scattering from each crack is minimal so that $\rho_c \ll 1$. The extra lag is designated X_i where the subscript indicates "independent" in the sense that there is no interaction with the other cracks in the array.
4. In Section 6, a map is given which shows the regime of validity for each of the preceding models.
5. In Section 7, the application of the analysis, with the aim of extracting the crack resistance ρ_c, from experimental measurements of phase lag and frequency is presented.
6. Finally, some concluding remarks are made in Section 8.

3. Thermal response at the periodic steady state

In this section, the exact solution for the thermal response, caused by a point source operating at the steady periodic state in an infinite cracked solid, is presented. First, a single unit cell is considered, and the so-called "cell transition matrix" [12,13], which relates the temperature and flux across a single cell, is found. Secondly, by cascading (multiplying) these matrices together, the temperature is found at any point within the solid. Special emphasis is placed on the temperature along the z axis.

3.1. Basic equations

The first unit cell is shown in Fig. 1(b). To construct the cell transition matrix it is noted that on either side of the crack the solid obeys the heat flow equation

$$\frac{\partial^2 T}{\partial r^2}+\frac{1}{r}\frac{\partial T}{\partial r}+\frac{\partial^2 T}{\partial z^2}=\frac{1}{\alpha}\frac{\partial T}{\partial t}. \tag{6}$$

On the surface $z=0$ the laser beam is focused to a vanishingly small spot of radius r_o and the flux is equal to the real part of

$$-k\left.\frac{\partial T}{\partial z}\right|_0=\frac{Q e^{i\omega t}}{\pi r_o^2}H(r_o-r), \tag{7}$$

where $H(r_o-r)$ is the step function and Q is the amplitude. The temperature is taken as the real part of the form

$$T(r,z,t)=e^{i\omega t}U(r,z). \tag{8}$$

Combining (6) and (8) the time dependence is removed so that $U(r,z)$ satisfies the reduced heat flow equation

$$\frac{\partial^2 U}{\partial r^2}+\frac{1}{r}\frac{\partial U}{\partial r}+\frac{\partial^2 U}{\partial z^2}=m^2 U, \tag{9}$$

where

$$m^2=\frac{i\omega}{\alpha}. \tag{10}$$

To proceed further it is convenient to: (i) remove the radial dependence by the use of a Hankel transform; (ii) solve the resulting ordinary differential equations to get the solution in the transformed space; and (iii) use the Hankel inversion to recover the radial dependence. The Hankel transform and its inverse are defined in standard texts, see for instance [14]:

$$\begin{aligned}\overline{U}(\beta,z)&=\int_{r=0}^{\infty}U(r,z)rJ_0(\beta r)\,dr,\\ U(r,z)&=\int_{\beta=0}^{\infty}\overline{U}(\beta,z)\beta J_0(\beta r)\,d\beta,\end{aligned} \tag{11}$$

where $J_0(\beta r)$ is a Bessel function of the first kind with order zero. For brevity the transformed quantity $\overline{U}(\beta,z)$ is written as $\overline{U}$. Using the properties of the Hankel transform the reduced heat equation (9) is transformed to the ordinary differential equation $d^2\overline{U}/dz^2-\gamma^2\overline{U}=0$ where

$$\gamma=\sqrt{\beta^2+m^2}. \tag{12}$$

The solution to the differential equation has the form $\overline{U}=Ae^{\gamma z}+Be^{-\gamma z}$ where the coefficients A and B are discontinuous on either side of the crack.

3.2. Cell transition matrix

The region $0<z<a/2$ is considered here as the "$-$" side of the cell. The transformed temperature is denoted by $\overline{U}_-(z)$ and its derivative $\overline{V}_-\equiv d\overline{U}_-/dz$ are given by

$$\begin{aligned}\overline{U}_-(z)&=A_1\exp(\gamma z)+B_1\exp(-\gamma z),\\ \overline{V}_-(z)&=\gamma A_1\exp(\gamma z)-\gamma B_1\exp(-\gamma z).\end{aligned}$$

The coefficients A_1 and B_1 are then found in terms of $\overline{U}(0)$ and $\overline{V}(0)$

$$\begin{Bmatrix}A_1\\B_1\end{Bmatrix}=\frac{1}{2\gamma}\begin{pmatrix}\gamma & 1\\ \gamma & -1\end{pmatrix}\begin{Bmatrix}\overline{U}(0)\\ \overline{V}(0)\end{Bmatrix}. \tag{13}$$

Similarly, on the "$+$" side of the crack, in the region $a/2<z<a$,

$$\begin{aligned}\overline{U}_+(z)&=A_2\exp(\gamma z)+B_2\exp(-\gamma z),\\ \overline{V}_+(z)&=\gamma A_2\exp(\gamma z)-\gamma B_2\exp(-\gamma z),\end{aligned}$$

so that transformed quantities are related to the coefficients by

$$\begin{Bmatrix}\overline{U}(a)\\ \overline{V}(a)\end{Bmatrix}=\begin{pmatrix}e^{\gamma a} & e^{-\gamma a}\\ \gamma e^{\gamma a} & -\gamma e^{-\gamma a}\end{pmatrix}\begin{Bmatrix}A_2\\B_2\end{Bmatrix}. \tag{14}$$

The crack is located at $z = a/2$ and the two boundary conditions across the crack are given by

$$\overline{V}_-(a/2) = \overline{V}_+(a/2) = \frac{h_c}{k}\left\{\overline{U}_+(a/2) - \overline{U}_-(a/2)\right\}. \quad (15)$$

These two conditions lead to

$$\left\{\begin{matrix} A_2 \\ B_2 \end{matrix}\right\} = \begin{pmatrix} 1 + \frac{\rho_c a\gamma}{2} & -\frac{\rho_c a\gamma e^{-\gamma a}}{2} \\ \frac{\rho_c a\gamma e^{\gamma a}}{2} & 1 - \frac{\rho_c a\gamma}{2} \end{pmatrix} \left\{\begin{matrix} A_1 \\ B_1 \end{matrix}\right\}. \quad (16)$$

Combining Eqs. (13), (14) and (16) it follows after matrix multiplication that

$$\left\{\begin{matrix} \overline{U}(a) \\ \overline{V}(a) \end{matrix}\right\} = \begin{pmatrix} \zeta & \eta\gamma^{-1} \\ \theta\gamma & \zeta \end{pmatrix} \left\{\begin{matrix} \overline{U}(0) \\ \overline{V}(0) \end{matrix}\right\}, \quad (17)$$

where the matrix terms are given by

$$\begin{aligned} \zeta &= \cosh a\gamma + \frac{\rho_c a\gamma}{2}\sinh a\gamma, \\ \eta &= \sinh a\gamma + \frac{\rho_c a\gamma}{2}(\cosh a\gamma + 1), \\ \theta &= \sinh a\gamma + \frac{\rho_c a\gamma}{2}(\cosh a\gamma - 1). \end{aligned} \quad (18)$$

The 2×2 square matrix in (17) is the cell transition matrix. It is convenient to designate this matrix by $\mathscr{C}$ so that (17) can be written in an abbreviated notation as $w_1 = \mathscr{C}w_0$ where w_0 and w_1 represent the column vectors in (17) and the subscripts represent the positions of the cell boundaries.

3.3. Cascading the cell transition matrices

Repetition of the same calculation on the second cell gives the thermal response at $z = 2a$ by the form $w_2 = \mathscr{C}w_1 = \mathscr{C}^2 w_0$. By further cascading the matrices, the thermal response at $z = na$ becomes

$$w_n = \mathscr{C}^n w_0. \quad (19)$$

Clearly it is useful to find an expression for the matrix $\mathscr{C}$ raised to integer powers. To begin this process the eigenvalues of $\mathscr{C}$ are found. It can be verified that $\det \mathscr{C} = \zeta^2 - \eta\theta = 1$ and therefore the product of the two eigenvalues, say μ_1 and μ_2, must equal unity, i.e., $\mu_1\mu_2 = 1$. The characteristic equation to find the eigenvalues is thus given by $\mu^2 - 2\zeta\mu + 1 = 0$ so that

$$\begin{aligned} \mu &= \mu_1 = \zeta + \sqrt{\zeta^2 - 1}, \\ \frac{1}{\mu} &= \mu_2 = \zeta - \sqrt{\zeta^2 - 1}. \end{aligned} \quad (20)$$

The two eigenvectors corresponding to μ_1 and μ_2 have the components $(\kappa_1, 1)$ and $(\kappa_2, 1)$ so that the standard equations can be written as

$$\begin{pmatrix} \zeta & \eta\gamma^{-1} \\ \theta\gamma & \zeta \end{pmatrix} \begin{pmatrix} \kappa_1 & \kappa_2 \\ 1 & 1 \end{pmatrix} = \begin{pmatrix} \kappa_1 & \kappa_2 \\ 1 & 1 \end{pmatrix} \begin{pmatrix} \mu_1 & 0 \\ 0 & \mu_2 \end{pmatrix}.$$

Using (20) along with $\zeta^2 - 1 = \eta\theta$ it is found that $\kappa_1 = -\kappa_2 = 1/\gamma\sqrt{\eta/\theta}$. The matrix $\mathscr{C}$ can then be expressed as

$$\begin{pmatrix} \zeta & \eta\gamma^{-1} \\ \theta\gamma & \zeta \end{pmatrix} = \begin{pmatrix} \kappa_1 & -\kappa_1 \\ 1 & 1 \end{pmatrix} \begin{pmatrix} \mu_1 & 0 \\ 0 & \mu_2 \end{pmatrix} \begin{pmatrix} \kappa_1 & -\kappa_1 \\ 1 & 1 \end{pmatrix}^{-1}$$

or, in abbreviated notation, $\mathscr{C} = \kappa\,\mu\,\kappa^{-1}$. In this form it is clear that

$$\mathscr{C}^n = (\kappa\,\mu\,\kappa^{-1})(\kappa\,\mu\,\kappa^{-1})\cdots(\kappa\,\mu\,\kappa^{-1}) = \kappa\,\mu^n\,\kappa^{-1}.$$

Since μ is a diagonal matrix the quantity μ^n is readily evaluated. It then follows that

$$\begin{aligned} \mathscr{C}^n &= \begin{pmatrix} \zeta & \eta/\gamma \\ \theta\gamma & \zeta \end{pmatrix}^n \\ &= \frac{1}{2}\begin{pmatrix} \mu_1^n + \mu_2^n & \sqrt{\eta/\theta}(\mu_1^n - \mu_2^n)/\gamma \\ \sqrt{\theta/\eta}(\mu_1^n - \mu_2^n)\gamma & \mu_1^n + \mu_2^n \end{pmatrix}. \end{aligned} \quad (21)$$

This is the desired result for the transition matrix raised to the integer power n.

3.4. Boundary conditions at $z = 0$ and $z = \infty$

Based on physical grounds it is clear that at a sufficiently large distance from the source both the temperature and flux die off so that $\overline{U}(na)$ and $\overline{V}(na)$ must tend toward zero as $n \to \infty$. The eigenvalues are given in (20) and $\mu_1 > 1$, $\mu_2 < 1$. Using Eq. (21) in (19), the transformed temperature $\overline{U}(na)$ can be found, and, when $n \gg 1$, is

$$\overline{U}(na) \sim \frac{\mu_1^n}{2}\left\{\overline{U}(0) + \sqrt{\frac{\eta}{\theta}}\frac{\overline{V}(0)}{\gamma}\right\}.$$

If $\overline{U}(na)$ is to vanish, the temperature and its derivative at $z = 0$, must be related by

$$\overline{U}(0) = -\frac{v}{\gamma}\overline{V}(0), \quad (22)$$

where

$$v = \sqrt{\eta/\theta}. \quad (23)$$

If $\overline{U}(0)$ and $\overline{V}(0)$ are not related in this way the temperature becomes infinite at large distances from the source. The heat input on the plane $z = 0$ is through a point (the circular area πr_o^2 in (7) is shrunk to a point), and taking the Hankel transform of (7) leads to an expression for $\overline{V}(0)$. Using this in conjunction with (22) gives

$$\left\{\begin{matrix} \overline{U}(0) \\ \overline{V}(0) \end{matrix}\right\} = \frac{Q}{2k\pi}\left\{\begin{matrix} v/\gamma \\ -1 \end{matrix}\right\}. \quad (24)$$

The transformed quantities at positions $z = na$ are thus found by using (24) in (19)

$$\overline{U}(na) = \frac{Q}{2k\pi}\frac{v}{\gamma}\mu^{-n},$$

$$\overline{V}(na) = -\frac{Q}{2k\pi}\mu^{-n}.$$

Finally, taking the inverse transform of $\overline{U}(na)$, the temperature is found

$$T(r, na, t) = \frac{Q\mathrm{e}^{\mathrm{i}\omega t}}{2k\pi}\int_0^\infty \frac{v}{\gamma}\mu^{-n}J_0(\beta r)\beta\,\mathrm{d}\beta, \tag{25}$$

where $z = na$. This integral represents the *exact* solution.

3.5. Temperature along the z axis

The temperature along the z axis is of special interest. At positions $z = na$ the complex temperature is given by

$$T(n) = \frac{Q\mathrm{e}^{\mathrm{i}\omega t}}{2\pi k}\int_0^\infty v\mu^{-n}\frac{\beta\,\mathrm{d}\beta}{\gamma}. \tag{26}$$

The point $z = 0$ coincides with the source so that the temperature $T(0) = \infty$ and the condition $n > 1$ is required for convergence. The nth cell is bounded by $(n-1)a < z < na$ and the thermal decrement across this cell is given by the ratio

$$\frac{T(n-1)}{T(n)} = \frac{\int_0^\infty v\mu^{-(n-1)}\beta/\gamma\,\mathrm{d}\beta}{\int_0^\infty v\mu^{-n}\beta/\gamma\,\mathrm{d}\beta} \equiv \exp\{\psi_n + \mathrm{i}\phi_n\}, \tag{27}$$

where the real part ψ_n gives the attenuation rate and the imaginary part ϕ_n gives the phase lag. The extra phase lag across the nth cell is thus given by

$$X(n) = \phi_n - p. \tag{28}$$

The extra lag $X(n)$ depends on $n = z/a$ and requires numerical evaluation.

To approximate these integrals, it is noted that the quantity $\mu^{-n} = \exp\{-n\ln\mu\}$ where $|1/\mu|$ is a decreasing function of β. For large values of n the integral is dominated by the behaviour near $\beta = 0$ so that it is then possible to use the Laplace type approximation [15] to evaluate the integral. In this method the integrand is expanded as a Taylor's series around $\beta = 0$, so that

$$\frac{v\mu^{-n}\beta}{\gamma} = \frac{v\exp\{-n\ln\mu\}}{\sqrt{m^2+\beta^2}}\beta \approx \mu_0^{-n}\exp(-n\mu_1\beta)\frac{(v_0 + v_1\beta\cdots)}{m\left(1+\frac{\beta^2}{2m^2}\right)}\beta,$$

where $\ln\mu \approx \ln\mu_0 + \mu_1\beta\cdots$ and $v \approx v_0 + v_1\beta\cdots$ represent the expansions around $\beta = 0$. Using these in (26) and retaining only the first order terms in β yields the result

$$T(n) \sim \frac{Q\mathrm{e}^{\mathrm{i}\omega t}}{2\pi km}v_0\mu_0^{-n}\int_0^\infty \mathrm{e}^{-n\mu_1\beta}\beta\,\mathrm{d}\beta = \frac{Q\mathrm{e}^{\mathrm{i}\omega t}}{2\pi km}\frac{v_0}{\mu_1^2}\frac{\mu_0^{-n}}{n^2}.$$

Thus as $n \to \infty$, the ratio $T(n-1)/T(n)$ approaches a constant value which is given by

$$\frac{T(n-1)}{T(n)} \sim \exp\{\psi + \mathrm{i}\phi\} = \mu_0 = \zeta_0 + \sqrt{\zeta_0^2 - 1}, \tag{29}$$

where the subscript "0" means that $\zeta_0 = \zeta(\beta = 0)$. Using (18) it follows that

$$\zeta_0 = \cosh\{am\} + \frac{\rho_c}{2}\{am\}\sinh\{am\}. \tag{30}$$

Using the standard identity $\ln(x + \sqrt{x^2-1}) = \cosh^{-1}x$, it is found that

$$\psi + \mathrm{i}\phi = \ln\mu = \cosh^{-1}\zeta_0 = \cosh^{-1}\left[\cosh\{am\} + \frac{\rho_c}{2}\{am\}\sinh\{am\}\right]. \tag{31}$$

The extra lag due to the presence of the crack approaches the limiting value given by

$$X = \phi - p. \tag{32}$$

This represents the asymptotic behaviour as the wave "flattens out". In other words, as the radius of curvature of the wave front becomes large in comparison with the crack spacing the thermal decrement across each cell becomes independent of n.

Fig. 2 shows a graph of $X(2)$, $X(6)$ and X versus p for various values of ρ_c ranging from 1/8 to 256. The values $X(2)$ and $X(6)$ were obtained by numerical evaluation of the integrals in (27). (The results for the cells $n = 3\ldots5$ were not shown to prevent clutter in the figure.) It is clear that $X(6)$ almost coincides with X over the entire frequency range. Considering the lag X, note the following features:

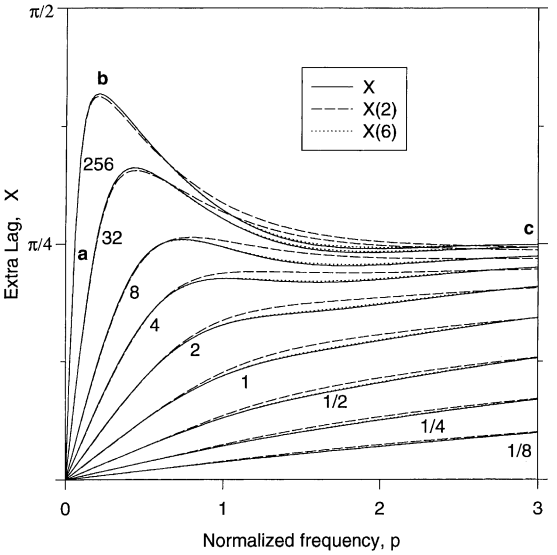

Fig. 2. Plot of $X(2)$, $X(6)$ and X versus p for values of $1/8 < \rho_c < 256$.

1. an initial linear portion, labelled "a", with slope $\{\sqrt{1+\rho_c}-1\}$, in agreement with (5);
2. the occurrence of a maximum for large values of ρ_c, shown at the labelled point "b" on the curve corresponding to $\rho_c = 256$;
3. as p becomes large, $X \to \pi/4$, corresponding to point "c";
4. for low values of ρ_c, the extra lag X shows no maximum value and all the results for $X(n)$ coalesce onto a single curve.

The slope in region "a" and the maximum point "b" are low frequency phenomena and are discussed in Section 4. The latter two phenomena are discussed in Section 5 with regard to the non-interacting model.

4. Low frequency behaviour

In this section, a simplified model for the low frequency behaviour is developed. If the crack spacing is sufficiently small, then it becomes reasonable to neglect the temperature variation in the z direction within the slab of solid residing between the cracks. Referring to Fig. 1(a), the nth slab is centered at $z = na$ and it occupies the region $na - a/2 < z < na + a/2$. The temperature T_n in the nth slab depends only upon r and is independent of z. The validity of this approximation of course depends upon the phase lag p and in this context $1/p^2$ is equal to the Fourier number for the cell. It is well known in the theory of heat conduction that to attain steady state requires large values for the Fourier number. Therefore if the z variation of temperature within the slabs is to be small then $p \ll 1$. In effect, the treatment is identical to the assumptions underlying the finite difference scheme where the mesh spacing Δz is set equal to the distance between cracks.

The thermal resistance of an area A across a unit cell is $R_{th} = a/Ak + 1/Ah_c$ so that k_z is given by (2). Therefore, the heat outflow per area from the nth slab to its two neighbours is $\Delta Q_z = -k_z(T_{n+1} - 2T_n + T_{n+1})/a$ and including the radial flow a heat balance leads to

$$\frac{\partial^2 T_n}{\partial r^2} + \frac{1}{r}\frac{\partial T_n}{\partial r} + \frac{k_z}{k}\left\{\frac{T_{n+1} - 2T_n + T_{n-1}}{a^2}\right\} = \frac{1}{\alpha}\frac{\partial T_n}{\partial t}. \quad (33)$$

As $a \to 0$ this second order difference equation tends to the heat flow equation for an anisotropic solid. The nth slab is centered at $z = na$ and the source is in the zeroth slab so that the flux boundary condition on $z = 0$, similar to (7), is expressed by the forward difference formula

$$\frac{k_z}{a}\{T_0 - T_1\} = \frac{Q e^{i\omega t}}{\pi r_o^2} H(r_o - r). \quad (34)$$

Near the source the temperature gradients are very large and the finite difference approximation is not particularly accurate. To eliminate the temporal component the temperature is written in the form

$$T_n = e^{i\omega t}\, U_n(r), \quad (35)$$

where $U_n(r)$ is a function of r. Using this form for T_n in (33) yields

$$(1+\rho_c)a^2\left\{\frac{\partial^2 U_n}{\partial r^2} + \frac{1}{r}\frac{\partial U_n}{\partial r}\right\} + \{U_{n+1} - 2U_n + U_{n-1}\} = 2i(1+\rho_c)n^2 U_n. \quad (36)$$

Taking the Hankel transform, given in (11), of this reduced heat equation gives the difference equation

$$\overline{U}_{n+1} - 2\overline{U}_n + \overline{U}_{n-1} = a^2\gamma^2(1+\rho_c)\overline{U}_n, \quad (37)$$

where $\overline{U}_n$ is the transform of U_n and $\gamma^2 = m^2 + \beta^2$ has been previously defined in (12). The solution to difference equations of this type are given in standard books, see for example [16], and in this case the solution has the form $\overline{U}_n = Be^{-n\epsilon}$. Using this in (37) after some algebra leads to

$$\epsilon = 2\sinh^{-1}\left\{\frac{a\gamma\sqrt{1+\rho_c}}{2}\right\}. \quad (38)$$

The transform of the boundary condition (34) is $\overline{U}_0 - \overline{U}_1 = Qa/2\pi k_z$ and this is used to find the constant B so that $\overline{U}_n$ is given by

$$\overline{U}_n(\beta) = \frac{Qa}{2\pi k_z}\frac{e^{-n\epsilon}}{1 - e^{-\epsilon}}.$$

Finally, application of the inverse Hankel transform (11) gives the temperature as

$$T_n = \frac{Qa e^{i\omega t}}{2\pi k_z}\int_0^\infty \frac{e^{-n\epsilon}}{1 - e^{-\epsilon}} J_o(\beta r)\beta\, d\beta. \quad (39)$$

4.1. Temperature along the z axis

Along the centerline it is possible to evaluate the integral in (39) by changing the variable of integration from β to ϵ. Using (38) it follows that $\gamma = \sqrt{m^2+\beta^2} = 2\sinh(\epsilon/2)/a\sqrt{1+\rho_c}$ and by the use of standard hyperbolic trigonometric identities

$$\beta\, d\beta = \frac{\gamma\cosh\epsilon/2\, d\epsilon}{a\sqrt{1+\rho_c}} = \frac{\sinh\epsilon\, d\epsilon}{a^2(1+\rho_c)}.$$

The lower limit of integration $\beta = 0$ corresponds to ϵ_0 which is given by

$$\epsilon_0 = 2\sinh^{-1}\left\{p\sqrt{\frac{i(1+\rho_c)}{2}}\right\}. \quad (40)$$

The upper limit $\beta = \infty$ corresponds to $\epsilon = \infty$ and the integral given in (39) reduces to the simple form

$$T_n = \frac{Q e^{i\omega t}}{4\pi a k} \int_{\epsilon_0}^{\infty} e^{-n\epsilon} \{e^{\epsilon} + 1\} \, d\epsilon. \tag{41}$$

As before, considering the behaviour when $n \gg 1$, the integral is dominated by its behaviour near the lower limit ϵ_0 so that the ratio

$$\frac{T_n}{T_{n+1}} = \exp\{\psi_\ell + i\phi_\ell\} \sim \exp\{\epsilon_0\} = \exp\left\{2\sinh^{-1}\left\{p\sqrt{\frac{i(1+\rho_c)}{2}}\right\}\right\},$$

where the subscript ℓ indicates "low" frequency. The phase lag ϕ_ℓ is then given by

$$\psi_\ell + i\phi_\ell = 2\sinh^{-1}\left\{p\sqrt{\frac{i(1+\rho_c)}{2}}\right\}, \tag{42}$$

where the phase lag ϕ_ℓ is the imaginary portion of the inverse hyperbolic sine on the right-hand side. The extra lag according to the low frequency model is then given by

$$X_\ell = \phi_\ell - \phi_0. \tag{43}$$

Fig. 3 shows a comparison between the exact value X given in (32) and X_ℓ for various values of ρ_c. For values of frequency

$$p < \frac{1}{3} \tag{44}$$

the low frequency model is in fairly good agreement with the exact result. Note two features: (i) the linear region

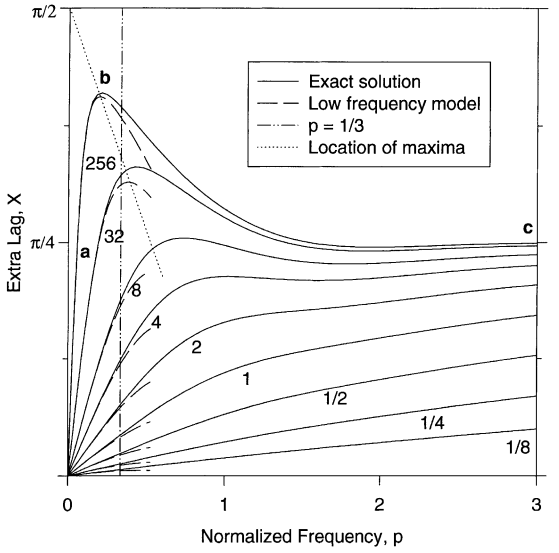

Fig. 3. Comparison of the low frequency model with the exact solution. For values $p < 1/3$, the low frequency model is in reasonable agree with the exact result. The approximate locus of maximum values is given by the line $X_m = \pi/2 - 3p/2$.

"a" near $p = 0$; and (ii) the existence of maxima for the curves where $\rho_c \gg 1$. These features are discussed below.

4.2. Transition to the equivalent solid

It is possible to establish an upper bound for p under which the equivalent solid model is valid. This situation corresponds to the case where the crack spacing "a" is made small enough, so that the difference equation given in (33) can be replaced by a partial differential equation which governs the thermal response of an equivalent anisotropic solid.

To begin, it is noted that for small values of x the inverse hyperbolic sine is given by $\sinh^{-1} x \sim x - x^3/6 + \cdots$ and therefore, considering (42) for small values of $p\sqrt{1+\rho_c}$ the inverse hyperbolic function can be approximated by the first term of its Taylor series. If $p\sqrt{1+\rho_c}$ is limited to values less than $1/3$ then $\phi_\ell \approx p\sqrt{1+\rho_c} < 1/3$. Since $\phi_0 = p$, it follows that $\phi_\ell = X_\ell + p$ and then

$$X_\ell + p \leqslant \frac{1}{3}. \tag{45}$$

his represents the regime in (p, X) space where the equivalent solid model is valid.

4.3. Maximum value of X_ℓ

Even for small values of p it is possible that the value of ρ_c is sufficiently large so that $\sqrt{1+\rho_c}p > \sqrt{2}$. For large values of its argument the Taylor series expansion of the inverse hyperbolic sine has the form $2\sinh^{-1} x \sim \ln 4x^2 + 1/2x^2 - \cdots$. The expression in (42) is then approximated by

$$\psi_\ell + i\phi_\ell = 2\sinh^{-1}\left\{p\sqrt{\frac{i(1+\rho_c)}{2}}\right\} \approx \ln\{2ip^2(1+\rho_c)\} - \frac{i}{p^2(1+\rho_c)}$$

and ϕ_ℓ is given by the imaginary part of the right-hand side. The extra lag is then given by

$$X_\ell \approx \frac{\pi}{2} - \frac{1}{(1+\rho_c)p^2} - p. \tag{46}$$

The derivative of X_ℓ with respect to p is designated X'_ℓ and the maximum value X_m corresponds to $X'_\ell = 0$. This occurs when

$$p = \left\{\frac{2}{1+\rho_c}\right\}^{1/3}. \tag{47}$$

The maximum value X_m is found by using this value of p in (46) to obtain

$$X_m \approx \frac{\pi}{2} - \left\{\frac{27}{4(1+\rho_c)}\right\}^{1/3} = \frac{\pi - 3p}{2}. \quad (48)$$

The line $X_m = \pi/2 - 1.5p$ is shown in Fig. 3 and, for values of $\rho_c > 8$, it gives reasonable estimates for the maxima. It is also clear that the maximum possible extra lag is always less than $\pi/2$.

5. Non-interacting cracks

As the thermal wave propagates through the solid, a portion of the wave is reflected at each crack while the remaining portion is transmitted. The reflected portion is subsequently back-reflected from neighbouring cracks thereby causing thermal interaction between cracks. This interaction becomes small if either: (i) the cracks are highly conductive so that $\rho_c \ll 1$ or, (ii) if the frequency is high enough so that $p \gg 1$. In the former case the perturbation to the thermal field is slight since the reflected portion is negligible. In the latter case the reflected portion attenuates so that the interaction is minimal. In many situations described in the literature the scattering obstacles are finite obstacles such as spheres or cylinders and it is often a reasonable approximation to neglect the secondary scattering [18,19] and accordingly the analysis simplifies. This situation is analogous to the mechanical stiffening of composites by second phase particles [17]. If the particles have approximately the same stiffness as the matrix then the interaction between them is small. Alternatively, in a dilute solution the particles are widely separated and regardless of their stiffness the interaction between them can neglected.

The object here is to develop an approximate model that simplifies the mathematics by neglecting the secondary scattering between cracks. To begin, consider the exact expression for the temperature which is given in (25) for values of $z = na$

$$T(r,z,t) = \frac{Q e^{i\omega t}}{2\pi k}\int_0^\infty v\mu^{-n} J_0(\beta r)\frac{\beta\,d\beta}{\gamma}. \quad (49)$$

The interaction is small either at sufficiently high frequency so that $|am| = \sqrt{2}p \gg 1$, *or* if the cracks offer little resistance, so that $\rho_c/2 \ll 1$. These two conditions can be described mathematically by the inequality

$$p + \frac{2}{\rho_c} \gg 1. \quad (50)$$

If (50) holds true and given that $\zeta = \cosh\{a\gamma\} + (\rho_c/2)\{a\gamma\}\sinh\{a\gamma\}$, it follows that the expression for the eigenvalue simplifies to

$$\mu \sim \zeta + \sqrt{\zeta^2 - 1} \sim e^{a\gamma}\left(1 + \frac{\rho_c a\gamma}{2}\right).$$

The parameter v given in (23) approaches unity and upon defining $\sigma \equiv 2/a\rho_c = 2h_c/k$, the integral in (49) reduces to

$$T(r,z,t) = \frac{Q e^{i\omega t}}{2\pi k}\int_{\beta=0}^\infty \left\{\frac{\sigma}{\sigma+\gamma}\right\}^n e^{-\gamma z} J_0(\beta r)\frac{\beta\,d\beta}{\gamma}, \quad (51)$$

Along the z axis, the temperature can be evaluated analytically in terms of the complementary gamma function $\Gamma(c,Z)$

$$T(n) = \frac{Q e^{i\omega t}}{2\pi k}\frac{e^{\sigma z}}{z}(\sigma z)^n \Gamma(1-n, zm + z\sigma),$$

where the complementary gamma function has the asymptotic behaviour

$$\Gamma(c,Z) = \int_Z^\infty e^{-t} t^{c-1} dt \sim Z^c \frac{e^Z}{Z} \quad \text{as } Z \to \infty.$$

Using the expression for σ, it follows that $|z(\sigma+m)| \approx n\{2/\rho_c + p\}$. In view of (50), the gamma function can be represented by its asymptotic form so that the temperature is given by

$$T(n) \sim \frac{Q e^{i\omega t}}{2\pi k}\frac{e^{-mz}}{z}\left\{\frac{\sigma}{\sigma+m}\right\}^n. \quad (52)$$

To find the lag across the nth cell it is necessary to consider the temperature ratio

$$\frac{T(n-1)}{T(n)} = \exp\{\psi_n + i\phi_n\} = \left\{\frac{n}{n-1}\right\} e^{am}\left\{1 + \frac{\rho_c}{2}am\right\}.$$

The extra lag due to the crack is equal to the argument of $(1 + \rho_c am/2)$

$$X_i = \arctan\left\{\frac{p}{p + (2/\rho_c)}\right\}, \quad (53)$$

where the subscript "i" indicates isolated or independent.

To obtain the range of validity for the non-interacting model suppose that the right-hand side of (50) is set equal to some value greater than unity. In fact, as discussed immediately below, using $p + 2/\rho_c \geqslant 3$ leads to a reasonable estimate for the validity range. Using this inequality in (53) it follows after some elementary algebra that

$$p \geqslant 3\tan X_i. \quad (54)$$

Fig. 4 shows X_i versus p for various values of ρ_c and as before the exact results obtained from (32) are also shown. The suggested validity range (54) gives the region in (p,X) space where the non-interacting model is valid. Note that if the crack conductance is low, i.e., $\rho_c < 2/3$ (approximately), the non-interacting model is valid for all values of p.

As a final point, it is noted that at sufficiently high frequencies, the extra lag $X_i \to \pi/4$, corresponding to

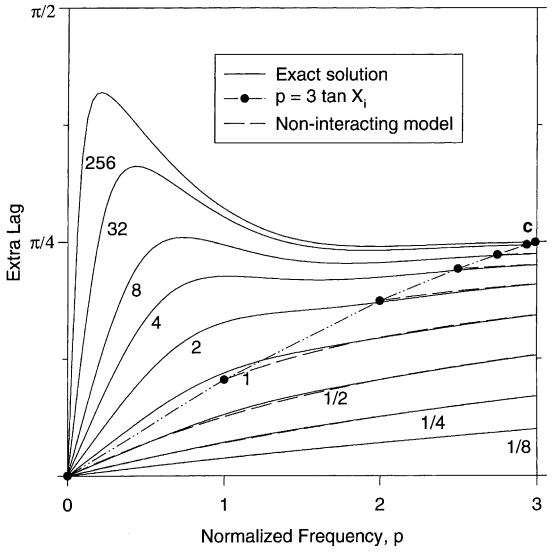

Fig. 4. Comparison of the non-interacting model with the exact solution. For $p \geqslant 3\tan X_i$, the non-interacting model is in good agreement with the exact model. The non-interacting model is universally valid when $\rho_c < 2/3$.

point "c" on Fig. 4. This can be rationalized in the following way. Since there is no interaction between cracks it is reasonable to consider an isolated crack that is positioned at $z = 0$. Let $T_-(z)$ and $T_+(z)$ represent the temperatures in the regions $z < 0$ and $z > 0$, respectively, and suppose that the periodic source is located somewhere in the region $z < 0$. The jump condition across the crack is given by

$$T_- = T_+ - \frac{k}{h_c}\frac{\partial T_+}{\partial z},$$

where T_- and T_+ are the temperatures on either side of the crack. At high frequencies the magnitude of $m = \sqrt{i\omega/\alpha}$ becomes large so that the derivative, $\partial T_+/\partial z \sim -mT_+$, where the negative sign accounts for the fact that T_+ decays as z increases. It then follows that $T_- \approx \{1 + mk/h_c\}T_+$. Eventually as the frequency is increased the magnitude of mk/h_c becomes large in comparison with unity and $T_- \sim \{mk/h_c\}T_+$. Since the phase angle of m is equal to $\pi/4$ it follows that T_+ lags T_- by this amount. In other words, there is a limiting phase lag of $\pi/4$ across the crack at high frequency. This discontinuity is not predicted by the equivalent solid model.

6. Regimes of validity for the simplified models

The extra lag $X(n)$ across a unit cell which is caused by the presence of the crack has been the focus of attention. As n increases, $X(n)$ rapidly approaches the limiting value X, and becomes $X(n)$ virtually independent of n when $z > 5a$. This is the regime of interest in the corresponding experimental study [7]. In this latter regime ($z > 5a$), the thermal response of the cracked body exhibits a variety of behaviors dependent on the normalized frequency p and the normalized crack resistance ρ_c. The exact solution for X is fairly complicated and simplified asymptotic models have been obtained to predict X. Their validity regimes have been established through comparisons with the exact numerical results.

At very low frequencies, the behaviour of the cracked solid is the same as that of an equivalent homogeneous anisotropic solid with the thermal conductivity tensor k_{ij} given in (3). Along the z axis, $X \sim X_e$ and varies linearly with p with a proportionality constant $\sqrt{1+\rho_c} - 1$. The validity range for X_e is $p + X < 1/3$ as given in (45). The equivalent solid model is a subset of the low frequency model which is valid over a wider frequency range, $p < 1/3$, as given in (44). The phase lag X_ℓ exhibits nonlinearity at higher frequencies and, for high values of $\rho_c (\gg 1)$, attains a maximum value that is always less than $\pi/2$.

The mathematical analysis becomes more straightforward if the secondary scattering is neglected. The extra lag X_i given in (53) is the prediction of the non-interacting model and the conditions where this model is reasonable have been discussed in Section 4. It has been shown in Fig. 4 that setting $p + \rho_c/2 > 3$ gives a reasonable estimate for the validity range and this validity regime can be equivalently expressed in (p, X) space by the inequality (54).

The regimes in (p, X) space in which the various models for X are valid are plotted in Fig. 5. The figure illustrates that the equivalent solid model (valid in the region denoted 0cef0) is a subset of the low-frequency

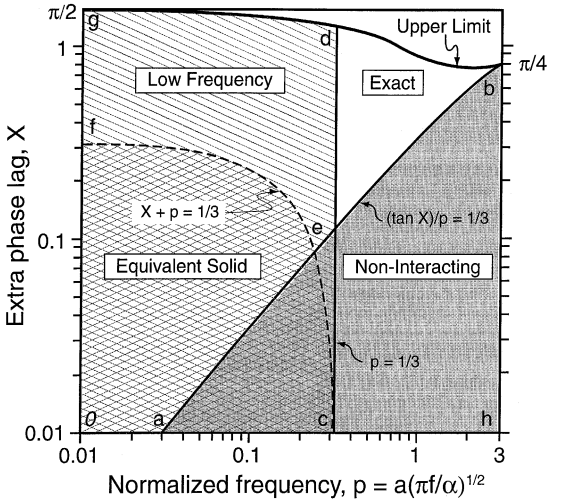

Fig. 5. Map showing the regimes of validity for the various models for X.

model (0cdg0). Furthermore, the non-interacting model is valid for a large portion of the high frequency regime and overlaps with the low frequency model in acea. The figure also shows that the exact numerical solution is only required in the region ebdb, defined by $p > 1/3$ and $p < 3\tan X$. The heavy line, gdb, gives the upper limit for the maximum possible extra lag due to the crack.

7. Application to experimental results

The aim of this section is to show how this calculation can be used to determine the value of ρ_c from experimental measurements. The experiments are performed by focusing a sinusoidally-modulated laser onto the surface of the sample, and, apart from the heat input due to the laser, the incident surface can be considered to be adiabatic. The preceding theoretical analysis gives the thermal response, caused by a point source, in an infinite solid containing a periodic array of cracks, and, provided that the thermal interactions from the other specimen surfaces are negligible, this analysis is applicable to the experiment. The effect of the other adiabatic specimen surfaces can sometimes, depending upon the symmetry of the specimen with respect to the cracks, be accounted for by the use of "image sources"; this effect is not considered here.

The thermal diffusivity, α, of the pristine material can be found by standard phase lag measurement, and α is regarded as a known quantity. After the cracks have been introduced, the laser is focused onto the specimen surface as shown in the inset of Fig. 6. The r,z axes are shown where the z axis is perpendicular to the cracks, and the phase lag Φ is measured over a distance, $\Delta z = z_2 - z_1$, which spans N cracks. A set of experimental data points, Φ and $P = \Delta z\sqrt{\pi f/\alpha}$, can thus be obtained. As previously discussed, when the distance z_1 becomes greater than about five times the crack spacing, the phase lag across each cell becomes uniform, and, for the sake of comparison with the results of Fig. 5, it is more useful to convert the points (P,Φ) into $(p,\phi) = (P,\Phi)/N$. The regimes in which the various models are valid are shown in Fig. 6. The lower limit, ϕ_0, corresponds to $\rho_c = 0$, and the line gdb represents the upper limit corresponding to $\rho_c = \infty$. All phase lag measurements must fall between these limits. The various regions are: (i) the equivalent solid model, which is bounded by $X + p = \phi - \phi_0 + p = \phi < 1/3$, and is valid in the region 0cf0 that is labelled "E"; (ii) the low frequency model, which is bounded by $p < 1/3$, and is valid in region 0cedgf0 that is labelled "Low"; and (iii) the non-interacting model, which is valid in region 0chae0, and is bounded by $p > 3\tan X = 3\tan(\phi - p)$. The dashed lines, showing ϕ versus p, are for the values of ρ_c given in the figure caption.

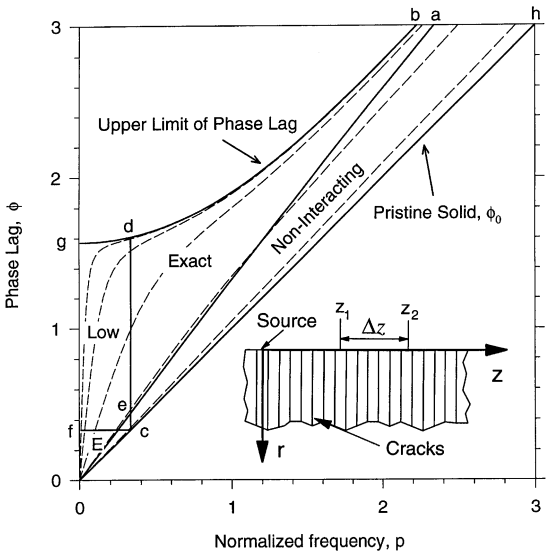

Fig. 6. Plot of ϕ versus p showing the regions where the various models are valid. The inset schematically illustrates the location of the source, the r,z axes, and the points z_1, z_2. The dashed lines show the behaviour of ϕ for values of $\rho_c = 0.1, 1, 10, 100$ and 1000. The line gdb corresponds to $\rho_c = \infty$, and point g represents $\phi = \pi/2$.

Consider a set of experimental points (P,Φ), obtained from a specimen having an unknown value of ρ_c. These points can be plotted on Fig. 6 by the transformation $(p,\phi) = (P/N, \Phi/N)$, and the aim is to find the value of ρ_c so that the calculated points (p,ϕ) fit the experimental data. The experimental data points that are in region E are the most simple to analyze; they fall on the line

$$\phi \approx p\sqrt{1+\rho_c}. \tag{55}$$

The determination of ρ_c from the experimental results then reduces to a straightforward linear fitting procedure. There are some experimental disadvantages to doing the measurements at very low frequencies: (i) the time taken to attain the steady-periodic state is long; (ii) a very small phase lag can be difficult to measure, and (iii) the rate of thermal attenuation becomes small, and, depending upon the specimen dimensions, the effect of the "reflections" off the boundaries can become significant. From an experimental viewpoint the situation can be somewhat ameliorated by considering the higher frequency data points, i.e., $p > 1/3$. If the crack resistance is not too large, say $\rho_c < 1$, then the non-interacting model becomes useful, and the expression for the phase lag is

$$\phi \approx p + \arctan\left\{\frac{\rho_c p}{\rho_c p + 2}\right\}. \tag{56}$$

This expression can be used to deduce ρ_c from the experimental measurements. In fact, as previously discussed, when $\rho_c < 2/3$ this expression for ϕ is valid at all frequencies. Moreover, when $\rho_c p \ll 1$, both Eqs. (55) and (56) give $\phi \sim (1 + \rho_c/2)p$. In contrast, if the crack resistance is large, $\rho_c > 1$, then the exact solution is required. Furthermore, as shown in the figure, for values of $\rho_c = 10,\ 100$ and 1000, the phase lag measurements tend to "run" together, approaching the line db, as p becomes large. Consequently, high frequency measurements are not useful for the determination of crack conductance when ρ_c is large.

In summary, it is clear that low frequency measurements made in the equivalent solid regime are the most straightforward to interpret. However, from an experimental viewpoint, it is sometimes preferable to make the measurements at higher frequency to eliminate thermal interaction due to the finite size of the specimen. If $\rho_c < 1$ then Eq. (56) gives a fairly simple relationship between ϕ, ρ_c and p, which can be used to extract the crack resistance ρ_c from a set of experimental measurements.

8. Concluding remarks

The analysis presented here is based on the assumption that the cracked solid has a structural periodicity in the z direction. The formation of the cell transition matrix requires a knowledge of the thermal properties of the pristine solid, plus the interface resistance, ρ_c. Although attention has been focused solely on the specific case where the heat input is periodic in time, other types of heat input can also be treated by using the same type of analysis, wherein, the cell transition matrices are cascaded. The application of the time-periodic analysis, to extract the crack resistance ρ_c from experimental phase lag measurements, has been a motivation for this work.

Acknowledgements

This material is based upon work supported by the US Office of Naval Research under Award No. N00014-97-1-0394 (Contract Officer: Dr. Steven G. Fishman).

References

[1] A. Mandelis, Principles and Perspectives of Photothermal and Photoacoustic Phenomena, Elsevier, New York, 1992.
[2] D.P. Almond, P.M. Patel, Photothermal Science and Techniques, Chapman & Hall, London, 1996.
[3] S.W. Indermuehle, R.B. Peterson, A phase sensitive technique for the thermal characterization of dielectric thin films, J. Heat Transfer – Trans. ASME 121 (3) (1999) 528–536.
[4] Y. Ohsone, G. Wu, J.R. Dryden, F. Zok, A. Majumdar, Optical measurement of thermal contact conductance between wafer-like thin solid samples, J. Heat Transfer – Trans. ASME 121 (4) (1999) 954–963.
[5] K.R. McDonald, J.R. Dryden, A. Majumdar, F. Zok, A photothermal technique for the determination of interfaces and cracks, J. Heat Transfer – Trans. ASME 122 (2) (2000) 10–14.
[6] K.R. McDonald, J.R. Dryden, A. Majumdar, F. Zok, Thermal conductance of delamination cracks in a fiber-reinforced ceramic composite, J. Am. Ceram. Soc. 83 (3) (2000) 553–562.
[7] K.R. McDonald, J.R. Dryden, F. Zok, Effects of matrix cracks on the thermal diffusivity of a fiber-reinforced ceramic composite, J. Am. Ceram. Soc., submitted.
[8] J.C. Maxwell, A Treatise on Electricity and Magnetism, vol. 1, Dover, New York, 1891, p. 446.
[9] S.J. Matysiak, A.A. Yevtushenko, E.G. Ivanyk, Temperature field in a microperiodic two-layered composite caused by a circular laser heat source, Heat and Mass Transfer 34 (1998) 127–133.
[10] A.A. Yevtushenko, S.J. Matysiak, E.G. Ivanyk, Influence of periodically layered material structure on the frictional temperature during braking, Int. J. Heat and Mass Transfer 40 (9) (1997) 2115–2122.
[11] H.S. Carslaw, J.C. Jaeger, in: Conduction of Heat in Solids, Oxford University Press, Oxford, 1959, p. 263.
[12] L.A. Pipes, Matrix solution of equations of the Mathieu–Hill type, J. Appl. Phys. 24 (1) (1953) 902–910.
[13] J.A. Richards, in: Analysis of Periodically Time-Varying Systems, Springer, Heidelberg, 1983, p. 413.
[14] I.N. Sneddon, in: The Use of Integral Transforms, McGraw-Hill, New York, 1972, pp. 298–352.
[15] C.M. Bender, S.A. Orszag, in: Advanced Mathematical Methods for Scientists and Engineers, McGraw-Hill, New York, 1978, pp. 261–267.
[16] H. Levy, F. Lessman, in: Finite Difference Equations, Dover, New York, 1961, pp. 94–99.
[17] J.D. Eshelby, The determination of the elastic field of an ellipsoidal inclusion, and related problems, in: Proceedings of the Royal Society of London: Series A, vol. 241, 1957, pp. 376–396.
[18] A. Mandelis, Theory of photothermal wave diffraction tomography via spatial Laplace spectral decomposition, J. Phys. A 24 (1991) 2485–2505.
[19] A. Sanchez-Lavega, A. Salazar, J.M. Terrion, A study of the photothermal signal produced by a series of subsurface cylinders in opaque materials, J. Appl. Phys. 84 (9) (1998) 5229–5237.